A stable compound of helium and sodium at high pressure

Xiao Dong[1,2,3], Artem R. Oganov[3,4,5,6]★, Alexander F. Goncharov[7,8], Elissaios Stavrou[7,9], Sergey Lobanov[7,10], Gabriele Saleh[5], Guang-Rui Qian[3], Qiang Zhu[3], Carlo Gatti[11], Volker L. Deringer[12], Richard Dronskowski[12], Xiang-Feng Zhou[1,3]★, Vitali B. Prakapenka[13], Zuzana Konôpková[14], Ivan A. Popov[15,16], Alexander I. Boldyrev[15] and Hui-Tian Wang[1,17]★

Helium is generally understood to be chemically inert and this is due to its extremely stable closed-shell electronic configuration, zero electron affinity and an unsurpassed ionization potential. It is not known to form thermodynamically stable compounds, except a few inclusion compounds. Here, using the *ab initio* evolutionary algorithm USPEX and subsequent high-pressure synthesis in a diamond anvil cell, we report the discovery of a thermodynamically stable compound of helium and sodium, Na$_2$He, which has a fluorite-type structure and is stable at pressures >113 GPa. We show that the presence of He atoms causes strong electron localization and makes this material insulating. This phase is an electride, with electron pairs localized in interstices, forming eight-centre two-electron bonds within empty Na$_8$ cubes. We also predict the existence of Na$_2$HeO with a similar structure at pressures above 15 GPa.

Helium is the second (after hydrogen) most abundant element in the universe and it is present in significant quantities in normal stars and in gas giant planets such as Jupiter and Saturn[1]. Helium and neon are the most inert elements in the periodic table. This is easy to understand as the ionization potential of the He atom (24.59 eV)[2] is the highest of all the elements and its electron affinity is zero[3]. In recent decades, many scientists have tried to find stable compounds of helium. The most successful example is the HeH$^+$ radical[4] (and, in general, He$_n$H$^+$ radicals, n = 1–6), which is stable only in its charged form, is extremely aggressive and protonates any base. All neutral molecules that have been found in theory or experiment, such as HHeF (ref. 5), (HeO)(CsF) (ref. 6) and LiHe (ref. 7), are metastable and very high in energy. For instance, HHeF has a computed energy more than 2 eV per atom higher than a mixture of HF molecules and He atoms. The only known stable solid compounds involving helium are van der Waals compounds such as NeHe$_2$ (ref. 8) and He@H$_2$O (ref. 9). For inclusion compounds, the enthalpy of formation is close to zero and removal of He atoms has little effect on the host's electronic structure.

Pressure greatly affects the chemistry of elements. For example, heavy noble gases become more reactive and form compounds with both electronegative and electropositive elements (for example, xenon oxides[10,11] and Mg–NG (NG = Xe, Kr, Ar))[12]. Metallic sodium, when subjected to a pressure of 200 GPa, becomes an insulator due to strong core–core orbital overlap, leading to interstitial valence electron localization[13]. Furthermore, unexpected compounds such as Na$_3$Cl, Na$_2$Cl, Na$_3$Cl$_2$, NaCl$_3$ and NaCl$_7$ (ref. 14) become stable under pressure. We therefore performed a large-scale evolutionary search for possible stable compounds of helium with a variety of elements (H, O, F, Na, K, Mg, Li, Rb, Cs and so on). We found that only Na readily forms a stable compound with He at pressures accessible to static experiments. In the following, we focus on the Na–He system.

Results and discussion

Stability and structures. Searches for stable compounds were performed using a variable-composition evolutionary structure prediction algorithm[15], as implemented in the USPEX code[16]. In such calculations, a phase is deemed stable if its enthalpy of formation from either elements or any other possible compounds is negative. Variable-composition structure searches were performed for the Na–He system at pressures of 0, 150, 200, 400, 700 and 1,000 GPa, allowing up to 36 atoms per primitive cell. We found a new compound, Na$_2$He (Figs 1 and 2), which has lower enthalpy than the mixture of elemental Na and He, or any other mixture, at pressures above 160 GPa (Fig. 1). The reaction

$$2\text{Na} + \text{He} \rightarrow \text{Na}_2\text{He} \qquad (1)$$

[1]School of Physics and MOE Key Laboratory of Weak-Light Nonlinear Photonics, Nankai University, Tianjin 300071, China. [2]Center for High Pressure Science and Technology Advanced Research, Beijing 100193, China. [3]Department of Geosciences, Stony Brook University, Stony Brook, New York 11794-2100, USA. [4]Skolkovo Institute of Science and Technology, 3 Nobel Street, Moscow 143026, Russia. [5]Moscow Institute of Physics and Technology, 9 Institutskiy Lane, Dolgoprudny city, Moscow Region 141700, Russia. [6]International Centre for Materials Discovery, Northwestern Polytechnical University, Xi'an 710072, China. [7]Geophysical Laboratory, Carnegie Institution of Washington, 5251 Broad Branch Road, Washington DC 20015, USA. [8]Key Laboratory of Materials Physics and Center for Energy Matter in Extreme Environments, Institute of Solid State Physics, Chinese Academy of Sciences, 350 Shushanghu Road, Hefei, Anhui 230031, China. [9]Lawrence Livermore National Laboratory, Physical and Life Sciences Directorate, PO Box 808 L-350, Livermore, California 94550, USA. [10]Sobolev Institute of Geology and Mineralogy, Siberian Branch Russian Academy of Sciences, 3 Pr. Ac. Koptyga, Novosibirsk 630090, Russia. [11]Istituto di Scienze e Tecnologie Molecolari del CNR (CNR-ISTM) e Dipartimento di Chimica, Universita' di Milano, via Golgi 19, Milan 20133, Italy. [12]Chair of Solid-State and Quantum Chemistry, RWTH Aachen University, Aachen D-52056, Germany. [13]Center for Advanced Radiation Sources, University of Chicago, Chicago, Illinois 60637, USA. [14]Photon Science DESY, Hamburg D-22607, Germany. [15]Department of Chemistry and Biochemistry, Utah State University, Logan, Utah 84322, USA. [16]Chemistry Department, Faculty of Science, RUDN University, 6 Miklukho-Maklaya Street, Moscow 117198, Russia. [17]Collaborative Innovation Center of Advanced Microstructures, Nanjing University, Nanjing 210093, China.
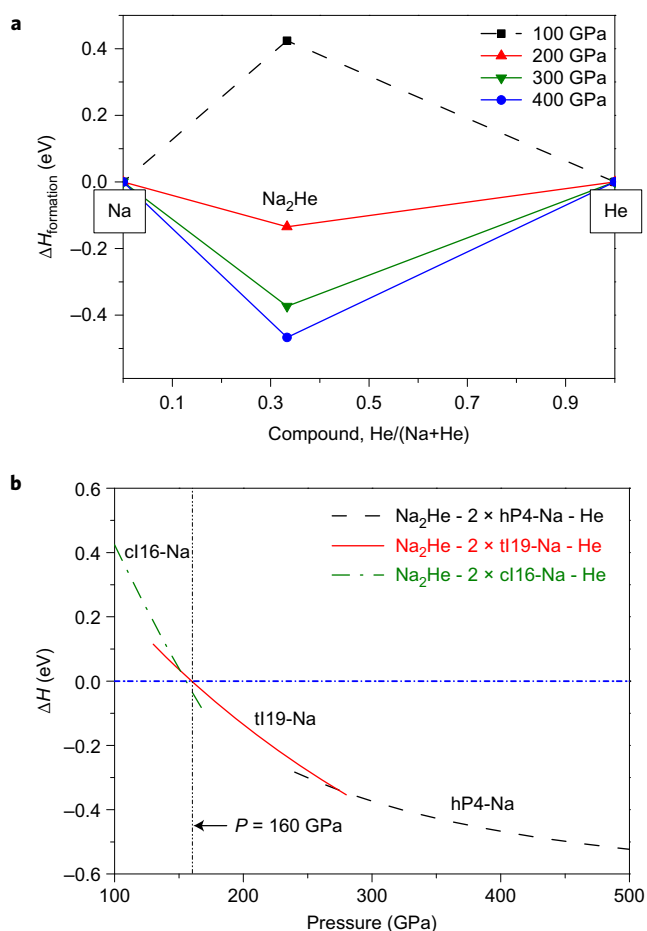*e-mail: artem.oganov@sunysb.edu; xfzhou@nankai.edu.cn; htwang@nankai.edu.cn

Figure 1 | Thermodynamics of the Na–He system, which shows the enthalpic stability between Na$_2$He and the mixture of elemental Na and He. a, Predicted convex hulls of the Na–He system, based on the theoretical ground states of Na and He at each pressure[13,18,22,50]. Here, $\Delta H_{formation}(Na_xHe_{1-x}) = xH(Na) + (1-x)H(He) - H(Na_xHe_{1-x})$, which can be considered as a criterion of thermodynamic stability. **b**, Enthalpy of formation of Na$_2$He as a function of pressure. Our calculated pressures of the cI16–tI19 and tI19–hP4 transitions of Na are 151 and 273 GPa, respectively, similar to previous calculations[13].

is predicted to be exothermic at pressures above 160 GPa, with reaction enthalpy as large as −0.51 eV at 500 GPa. Phonon calculations clearly indicate dynamical stability of Na$_2$He above 100 GPa (Supplementary Fig. 1). This means that, once formed,

this phase can be quenched down to 100 GPa, but at and below 50 GPa it is dynamically unstable and therefore unquenchable to ambient conditions. Quasiharmonic free energy calculations suggest that temperature has little effect on the Gibbs free energy of formation of Na$_2$He: for example, it increases from −0.41 eV at 0 K to −0.39 eV at 800 K at 300 GPa (Supplementary Fig. 2).

Na$_2$He becomes stable at a pressure near the cI16–tI19 transition of elemental Na (we also observed this in experiments, see section 'Experiments'). The transition in Na has an underlying electronic stabilization mechanism related to the development of a pseudogap or gap at the Fermi energy (tI19 is a very poor metal and hP4, the phase appearing with a further increase in pressure, is an insulator[13]). This hints at a possible electronic stabilization of Na$_2$He, which has a surprisingly wide bandgap in the entire pressure range of its stability. Insulating Na$_2$He is predicted to form at a lower pressure than insulating hP4-Na (160 versus 273 GPa). The transition pressure for hP4–Na is significantly overestimated (the experimental value is 195 GPa; ref. 13). Density functional theory (DFT) is known to underestimate the stability fields of systems with localized electronic states, and it is expected that Na$_2$He will similarly become stable at pressure below the theoretical estimate of 160 GPa.

Na$_2$He has only one ground-state structure (Fig. 2) in the whole pressure range explored here (that is, from 160 to 1,000 GPa). There are several equivalent ways to describe it. (1) Considering only the positions of the atoms, this is a fluorite-type structure, a three-dimensional checkerboard with alternating He-filled and empty cubes formed by the Na atoms. However, the fluorite structure is not dense, and in all known compounds becomes unstable even at moderate pressures[17]. (2) Just like hP4–Na (ref. 13), Na$_2$He is an electride, that is, an ionic crystal with a strong Madelung field and an interstitially localized electron (actually, an electron pair in both hP4–Na and Na$_2$He) playing the role of the anion. If one also considers the positions of localized electron pairs (2e$^-$), this is a topologically very dense Heusler alloy structure (AlCu$_2$Mn-type, related to the Fe$_3$Al-type), where He atoms form a cubic close packing, in which all tetrahedral voids are filled by the Na atoms and 2e$^-$ fill all octahedral voids. Every He atom (and every 2e$^-$) is coordinated by eight Na atoms. Note that the 2e$^-$ form a cubic close packing of their own, and in hP4–Na, they form a nearly perfect hexagonal close packing[13]. (3) This structure can also be viewed as an ordered body-centred cubic (bcc) superstructure formed by Na, He and 2e$^-$.

Experiments. In the present experiments, Na was loaded into a He medium in a laser-heated diamond anvil cell (DAC) and compressed up to 155 GPa (Supplementary Table 1). The sample was monitored using synchrotron X-ray diffraction (XRD), Raman spectroscopy and visual observations. The latter verified (Supplementary Fig. 3) that there was He in the DAC high-pressure cavity, as there were
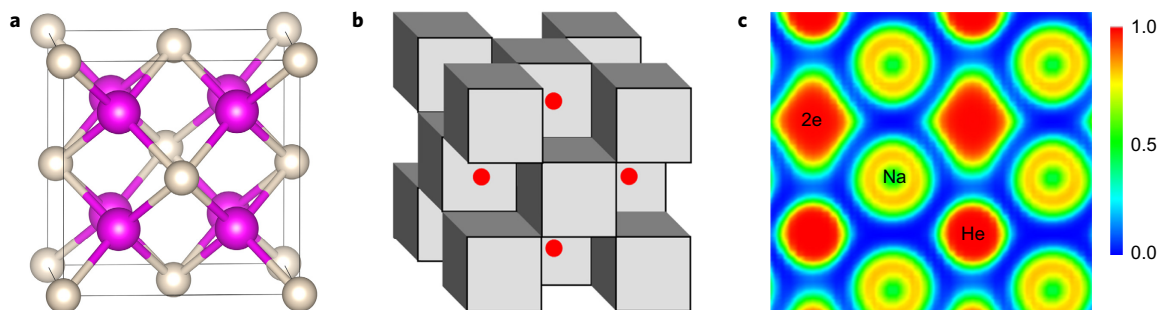

Figure 2 | Crystal structure of Na$_2$He at 300 GPa. a,b, Ball-and-stick representation (**a**, pink and grey atoms represent Na and He, respectively) and polyhedral representation (**b**), where half of the Na$_8$ cubes are occupied by He atoms (shown as polyhedra) and half by 2e (shown as red spheres). **c**, Electron localization function (ELF, which measures the spatial localization of electrons) plotted in the [110] plane at 300 GPa. This structure has space group *Fm-3m* with lattice parameter $a = 3.95$ Å at 300 GPa and Na atoms occupying the Wyckoff position 8c (0.25,0.25,0.25) and He atoms occupying the 4a (0,0,0) position.
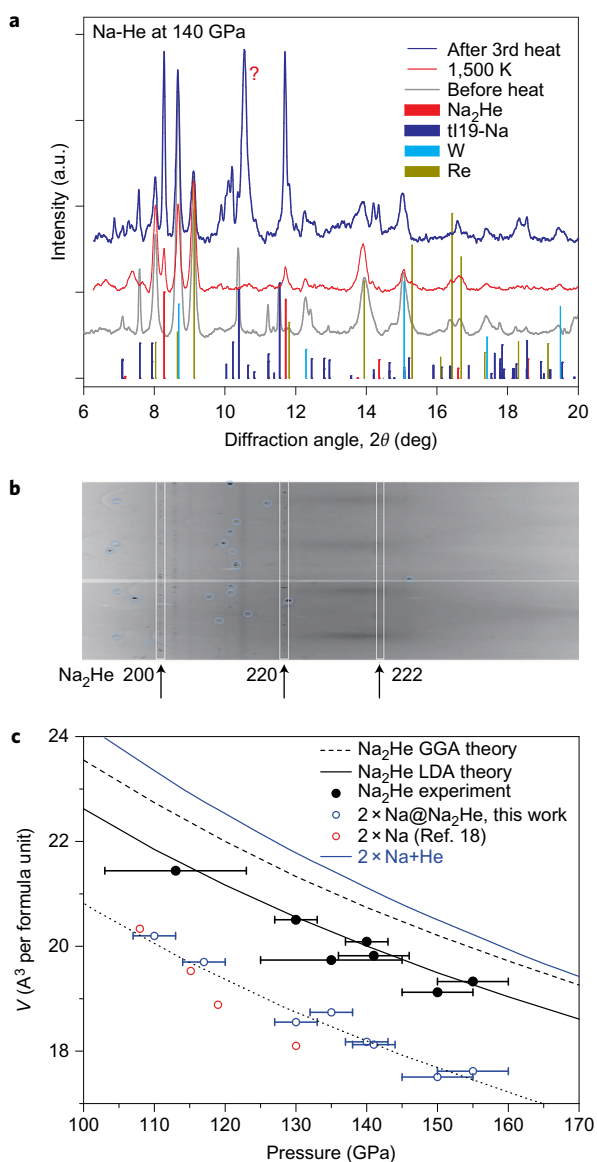
Figure 3 | Experimental data on Na$_2$He: XRD at 140 GPa. a, Integrated XRD patterns before heating and after the second and third heating to ~1,200 and >1,500 K, respectively. Vertical ticks correspond to expected positions and intensities of XRD peaks of Na$_2$He, tI19-Na (ref. 18), Re (gasket) and W (pressure gauge). **b**, Two-dimensional image after the third heating, in radial coordinates, showing single-crystal reflections of tI19-Na and Na$_2$He, marked by light blue circles and white rectangles, respectively. This pattern was obtained during a continuous rotation of the DAC along the ω axis to collect as many single-crystal reflections of tI19-Na as possible. Semi-continuous lines are from the Re gasket. Diffraction from Na$_2$He and W consists of many small, almost uniformly spaced spots. After the third heating, a new almost continuous line appeared near 10.5°, which we assigned to yet unidentified reaction products. The X-ray wavelength is 0.31 Å. **c**, Equation of state (EOS) of Na$_2$He synthesized in a DAC at 113–155 GPa in comparison with the EOS of Na. Filled circles: experimental unit cell volumes of Na$_2$He. Open blue circles: volumes per two Na atoms. Error bars correspond to the experimental pressure uncertainty due to pressure gradients and pressure measurements. Pressure was determined from XRD measurements of the W marker in one experiment and using Raman shift of the stressed diamonds[51]. The solid blue line corresponds to a superposition of the EOS of Na and He (2Na + He) determined from experimental data[52]. Dashed and solid lines are the results of our GGA and LDA calculations, respectively. Dotted line: extrapolated EOS of fcc Na from ref. 19. Open red circles: volumes of Na phases reported in ref. 18.

transparent colourless areas around the Na sample, which remained up to the highest pressure reached. Below ~110 GPa, only single-crystal reflections of elemental Na were observed in XRD and their positions agreed with previously reported structural data and the equation of state (EOS)[18,19]. Above 113 GPa, we detected the appearance of new single-crystal reflections, which became stronger after laser heating to $T > 1,500$ K. On further compression, unreacted Na (which remains dominant) in the quenched sample showed the transition sequence cI16–oP8–tI19 characteristic of Na at $P > 113$ GPa (ref. 18). At $P > 140$ GPa, the transformation to the tI19 phase was complete. Prolonged heating at 140 GPa yielded quasi-continuous diffraction lines (Fig. 3a,b), revealing substantial production of a new phase. Our laser heating experiments confirmed that compressed Na has a low melting temperature, slightly above 300 K near 120 GPa (refs 18, 20). Heating close to the melting temperature of He (~1,500 K)[21] yields more reaction product and the yield increases during further heating.

New reflections were assigned to the predicted fluorite-type Na$_2$He (Fig. 3a,b). They can be indexed in a cubic structure based on their positions and relative intensities (Supplementary Table 2), with lattice parameter in good agreement with theory (Fig. 3c). Experiments show that Na$_2$He has a much higher melting point than pure Na, perhaps above 1,500 K at 140 GPa (Fig. 3a,b), whereas pure sodium melts slightly above 550 K (refs 20, 22), indicating very different energy landscapes and bonding types in Na and Na$_2$He. Experiments confirmed the stability of Na$_2$He, as it is denser than the mixture of Na and He (Fig. 3c) and crystallizes from a sodium–helium melt. Our experiments traced this phase on decomposition down to 113 GPa and its volume–pressure dependence is in good agreement with theoretical predictions (Fig. 3c). The increased yield of the new phase after laser heating (Fig. 3a,b) indicates that a low yield of Na$_2$He at near room temperature is due to kinetic hindrance for the Na (fluid)–He (solid) reaction. Raman experiments on samples quenched to 300 K (Supplementary Fig. 4) showed the presence of a new broad weak peak at 470 cm^{-1} in addition to peaks that can be assigned to tI19-Na (ref. 20).

Chemical bonding. Having experimentally confirmed the stability of this compound, we wished to understand its origin. By analogy with other noble gases, one could expect helium to rather form stable compounds with the most electronegative atoms, or perhaps with molecular entities such as H$_2$ (for example, Xe forms stable fluorides under ambient conditions, stable oxides under pressure[11] and compounds with H; ref. 23). However, due to its extremely high ionization potential, the highest among all elements, helium does not react with oxygen or fluorine even at the extremely high pressure of 800 GPa. Xenon was predicted to react with electropositive elements (for example, with Mg; ref. 12) under pressure, but in contrast to Xe, He has zero electron affinity and is much less reactive. So what is the chemical nature of Na$_2$He?

It can be easily demonstrated that Na$_2$He is not an inclusion compound. The formation of inclusion compounds involves little electronic redistribution, and host–guest interaction has only a moderate effect on physical properties. Na$_2$He is very different. Its formation is strongly exothermic and its Na sublattice has a simple cubic structure with one valence electron per unit cell and must be metallic. However, upon insertion of He a wide bandgap opens up (Fig. 4). Electronic redistribution due to the insertion of He into the simple cubic sodium sublattice (Fig. 4) is also very large, again proving that this is not an inclusion compound. We observe a contraction of charge density towards all nuclei, but the main effect is its removal from the region occupied by helium and strong buildup in the empty Na$_8$ cubes. Strong non-nuclear charge density maxima allow us to call this compound an electride[24,25].

Na$_2$He and hP4-Na differ fundamentally from the known low-pressure electrides[26], where interstitially localized electrons are
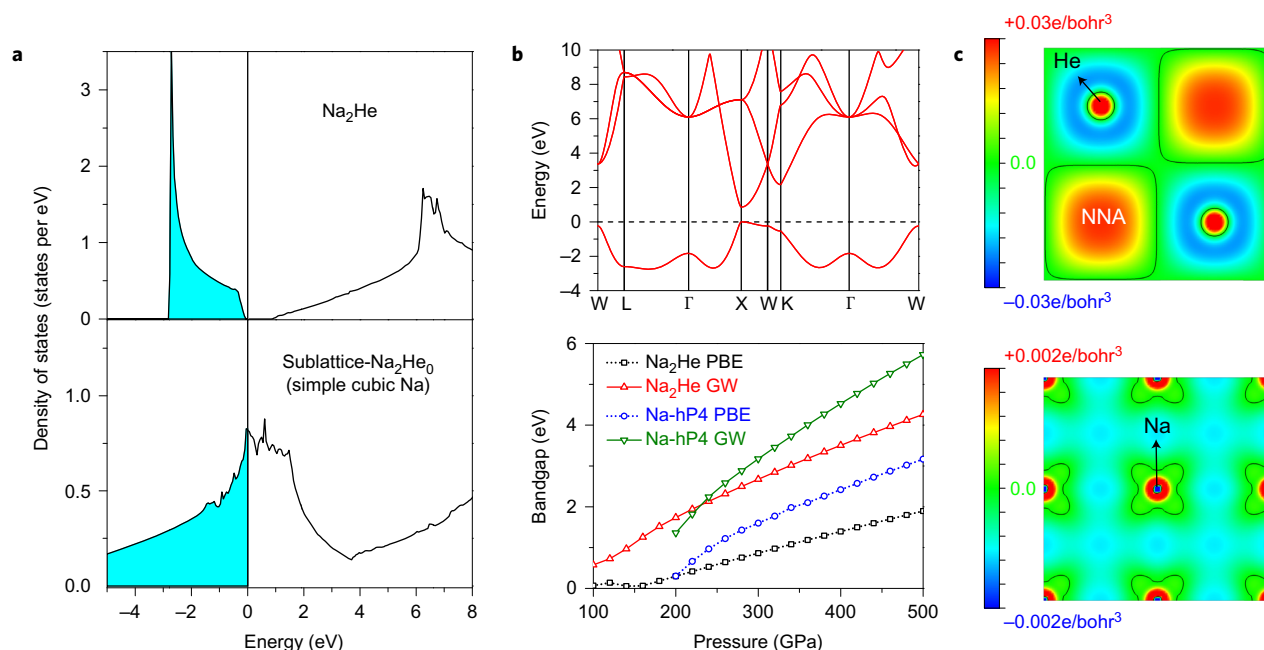
Figure 4 | Electronic structure of Na₂He. a, Density of states (DOS) of Na₂He and its Na-sublattice, showing that the insertion of He opens a bandgap (the pure Na sublattice is metallic). The vertical line is the Fermi level. **b**, Band structure and bandgap as a function of pressure. GW gaps (where G is the Green's function and W is the screened Coulomb interaction) are typically accurate to within 5–10% of experimental values[53]. It shows that both Na and Na₂He have a wide gap that increases with pressure. **c**, Electron density change (defined as $\rho(Na_2He)-\rho(Na\ sublattice)-\rho(He\ sublattice)$) induced by insertion of the He sublattice. (100) sections passing through He atoms (above) and Na atoms (below) are shown at 300 GPa. NNA (non-nuclear attractors) corresponds to interstitial electron localizations. The insertion of He pushes electron density out, causing its interstitial localization.

unpaired and spin-polarized. Spin pairing increases the density, making electron-paired electrides a novel type of compound, which are stable under pressure. Valence and conduction bands are expected to broaden under pressure, leading to gap closure and pressure-induced metallization (Wilson model). However, both hP4-Na and Na₂He display the opposite behaviour: they are insulating throughout their stability fields, with bandgaps increasing under pressure (Fig. 4b). With direct bandgaps exceeding 1.8 eV at pressures above ~200 GPa, both Na₂He and hP4-Na are expected to be optically transparent, and for hP4-Na, this prediction has been confirmed experimentally[13]. In our experiments, optical transparency of Na₂He could not be checked because of the presence of unreacted Na shielding the transmitted light. Theoretically, Na₂He has an even wider gap than hP4-Na at pressures below 230 GPa. Interstitial localization of valence electrons can be viewed as a result of overlap of the core and valence orbitals of neighbouring atoms, forcing valence electrons into the voids of the structure. At 300 GPa, the Na–Na distance is 1.98 Å, shorter than twice the core radius[27] (2.04 Å) of the Na atom. Compression leads to further localization of the interstitial electron pair, band narrowing and opening of the bandgap[28]. Quantum mechanics predicts that interstitial electron pairs, once localized in space, will tend to adopt a spherical shape to minimize their kinetic energy, and our calculations indeed show nearly spherical electron localizations (Supplementary Fig. 5), characterized by volumes and radii, as normal atoms.

We can take the electride description one step further, considering Na₂He to be a special kind of ionic crystal, stable because it satisfies Pauling's rules[29] for ionic structures. Pauling's first rule is satisfied here: the ratios of the radii (defined as the shortest distance to the Bader boundary[30,31]), $r_{He}/r_{Na} \approx 0.83$ and $r_{2e}/r_{Na} \approx 0.75$, are compatible with eightfold coordination (which requires ratios >0.732). A favourable atomic size ratio r_{He}/r_{Na}, alone, is not sufficient to stabilize this compound. We find that although the r_{Ne}/r_K ratio under pressure is closer to the ideal 0.732 for eightfold coordination (Supplementary Figs 6 and 7 and Supplementary Table 3), all

K–Ne compounds are massively unstable. Taking into account the positions and charges of '2e⁻', Na₂He also satisfies Pauling's second rule (local electrostatic balance), while hP4-Na does not satisfy it, explaining why Na so readily reacts with He to form Na₂He at high pressure.

The Bader charges[30] (Supplementary Table 5) of Na atoms in both hP4-Na and Na₂He are close to +0.6, He atoms in Na₂He have a small negative charge (~−0.15e), while charges of '2e⁻' are close to −1.1. For comparison, charge transfer in the inclusion compound He@H₂O (ref. 9), predicted at ultrahigh pressures, is just 0.03e. Further insight can be obtained by considering the change in the properties of Bader atoms upon the formation of Na₂He from the elements (Table 1). Below 300 GPa, all stabilization is due to volumetric gain (PV term in enthalpy), whereas above 300 GPa, energetic stabilization also comes into play. Table 1 shows large changes in the atomic energies as a result of electronic redistribution at 300 GPa. Although He atoms expand and lower their energy, all the other atomic basins shrink and their energy increases. The balance of different factors is quite complex, the greatest stabilizing factors being the decrease in the energy of the He atoms by 11.515 eV and shrinking of 2e⁻ (PV decrease of 0.966 eV).

We performed a simple computational experiment, taking a large face-centred cubic (fcc) supercell of He and replacing one He atom with Na, as in refs 24 and 25. We found that at pressures of ~80 GPa, occupied Na–3s (HOMO) and empty He–2s (LUMO) energies become equal, enabling orbital mixing (Supplementary Fig. 11) and some charge transfer from Na–3s to He–2s.

Further insight is provided by advanced methods such as solid-state adaptive natural density partitioning (SSAdNDP)[32,33] and periodic natural bond orbital (NBO) methods[34,35] (Supplementary Table 6) and integrated crystal orbital Hamilton populations (ICOHP)[36,37] (Supplementary Fig. 10). SSAdNDP and NBO show small, but puzzling, charge transfer from He–1s to Na–3p, and more expected transfers from He–1s to He–2s and from Na–3s to Na–3p orbitals with increasing pressure. ICOHP shows that Na–Na and especially Na–2e⁻ (but not Na–He and He–2e⁻) are the only important

Table 1 | Change in atomic properties integrated over Bader basins for reaction (1) at 300 GPa.

	Total	Na1	Na2	He	2e
ΔN	0.000	0.007	−0.067	0.151	−0.094
ΔV (Å³)	−0.207	−0.130	−0.216	0.644	−0.516
$P\Delta V$ (eV)	−0.388	−0.244	−0.405	1.206	−0.966
ΔE (eV)	−0.018	3.090	7.764	−11.515	0.642

N, number of electrons; *V*, atomic volume; *E*, atomic energy.

interactions and they are both bonding direct covalent interactions. This conclusion is consistent with the SSAdNDP and NBO analyses, where all electron density is assigned to the atoms, and electron pairs occupying empty Na_8 cubes emerge as eight-centre two-electron (8c–2e) bonds. These bonds are formed by sp^3-hybridized atomic orbitals of sodium as derived from the NBO method[34,35]. If one considers only the Na sublattice, on average there is just one electron located in every Na_8 cube. On insertion of He into half of all Na_8 cubes to form Na_2He, He atoms push the electron density out of the filled Na_8He cube and into the neighbouring empty Na_8 cube, enhancing the formation of 8c–2e bonds. Even at 0 GPa, He pushes out ~0.4 |e| from its cube, which helps to form the 8c–2e⁻ bond with an occupation number (ON) of 1.40 |e| inside the neighbouring empty cube. There are still about 0.6 |e|, which can be found in the Na_8He cube. With increasing pressure, He continues to push out the remaining electron density into the empty Na_8 cube, increasing the ON of the 8c–2e bond to 1.80 |e| at 100 GPa, 1.88 |e| at 300 GPa and finally to 1.89 |e| at 500 GPa (Supplementary Table 6). This eight-centre two-electron bonding is essential for the stability of Na_2He. A complementary view of this is that Na_2He is an ionic salt (electride), stable thanks to long-range electrostatic interactions and a crystal structure that is in perfect harmony with the electronic redistribution.

Na is a light alkali metal and is less reactive than the heavier K, Rb and Cs at ambient pressure. Yet, our calculations show the absence of thermodynamically stable K–He, Rb–He and Cs–He compounds at pressures below 1,000 GPa. For Li, we do find that Li_5He_2 becomes stable at 780 GPa. The difference between light (Li and Na) and heavy (K, Rb and Cs) alkali metals has been discussed by Winzenick and colleagues[38]: only heavy alkalis under pressure undergo an $s \rightarrow d$ electronic transition, making them 'incipient transition metals'. For example, the electronic configuration of K changes from $[Ar]4s^1$ to $[Ar]3d^1$ and the $3d$ electron will be rather localized and able to penetrate the core, explaining the reduced reactivity and absence of stable K–He compounds. Under pressure, Na paradoxically has lower electronegativity and higher reactivity than K. Indeed, we find that in A–He and A–Ne (A=Na, K) systems under pressure, Na compounds have much lower enthalpies of formation (for example, Supplementary Fig. 6). The high reactivity of compressed Na is due to the interstitial electron pair and is consistent with what is known about electrides—that they have extremely low work functions and can be used as powerful reducing agents[39]. It is very interesting that, according to our calculations (and consistent with the properties of known low-pressure electrides), the insulating electride phase of Na is more reactive than metallic Na. Li is only a weak electride, whereas heavier alkali metals (K, Rb and Cs) are not electrides and are less reactive under pressure.

Na_2HeO. With this in mind, we hypothesized that Na_2He, with a bare interstitial electron pair, might be stabilized by a strong acceptor of an electron pair—for example, oxygen[40]. Our structure searches showed that Na_2O, indeed, has the same structure as hP4-Na, and Na_2HeO is isostructural with Na_2He. In both cases, O^{2-} (that is, oxygen with the absorbed electron pair) occupies the position of '2e⁻' and both can be considered as salts. Importantly, Na_2HeO is thermodynamically stable in the Na–He–O system in the pressure range 15–106 GPa.

Conclusions

In conclusion, a systematic search for stable compounds of helium has resulted in the prediction and experimental verification of a cubic-phase Na_2He, stable from 113 GPa up to at least 1,000 GPa. This phase is an electride, that is, a crystal made of positively charged ionic cores and with strongly localized valence electrons playing the role of anions. The insertion of He atoms pushes away the electron gas, leading to localization of valence electrons and the formation of eight-centre two-electron bonds and opening of a wide bandgap, just as for a salt-like compound. The predicted two compounds, Na_2He and Na_2HeO, change the hitherto bare field of helium chemistry, provide new twists to the chemistry of noble gases, and will have an impact on our understanding of chemical bonding and of the chemical processes that occur inside giant planets.

Methods

Theory. The evolutionary algorithm USPEX[16], used here for predicting new stable structures, searches for the lowest-enthalpy structures at a given pressure, and is capable of predicting stable compounds and structures knowing just the chemical elements involved. A number of applications[11,13,14,16,41] illustrate its power. Structure relaxations were performed using DFT within the Perdew–Burke–Ernzerhof (PBE) functional[42] in the framework of the all-electron projector augmented wave (PAW) method[43], as implemented in the VASP code[44]. For Na atoms we used PAW potentials with 1.2 a.u. core radius and $2s^2 2p^6 3s$ electrons treated as valence. For He the core radius was 1.1 a.u. and $1s^2$ electrons were treated as valence. We used a plane-wave kinetic energy cutoff of 1,000 eV and the Brillouin zone was sampled with a resolution of $2\pi \times 0.06$ Å^{-1}, which showed excellent convergence of the energy differences, stress tensors and structural parameters. The first generation of structures was created randomly. All structures were relaxed at constant pressure and 0 K and the enthalpy was used as fitness. The energetically worst structures (40%) were discarded and a new generation was created, 30% randomly and 70% from the lowest-enthalpy structures through heredity, lattice mutation and transmutation.

To obtain atomic properties (Bader charges, atomic volumes and atomic energies), perform critical point analysis, compute Mulliken charges and deformation density maps, we performed all-electron calculations using the CRYSTAL14 code[45]. Triple-zeta quality Gaussian basis sets were used for all atoms, including also basis functions centred on non-nuclear charge density maxima positions, which are the centres of interstitial electron localizations (details of the basis set and grid used to sample direct and reciprocal space are reported in section 'Supplementary Methods'). The topological properties of charge density were obtained using the TOPOND code[46] incorporated into CRYSTAL14. Bader volumes and charges were also obtained using VASP and code from ref. 31, and the results are essentially identical to those obtained using CRYSTAL14. Crystal orbital Hamilton population (COHP) analysis[36] was performed using periodic localized orbitals as implemented in the TB-LMTO-ASA framework[47]. We also explored the effects of temperature on stability using the quasiharmonic approximation, for which phonon calculations were performed for all relevant structures using the PHONOPY code[48]; for each structure, phonons were computed at 20 different volumes to predict the Gibbs free energy.

Experiment. We loaded thin Na (3–5 μm) plates (30 × 30 μm² dimensions) in a DAC cavity (30–40 μm diameter) made in indented to 20 μm thickness rhenium gasket in a glove box and then filled the rest of the cavity with He gas compressed to 1,600 bar. Diamond anvils with 70–100 μm central tips bevelled to a 300 μm outside culet diameter were used. Synchrotron X-ray diffraction was monitored on increasing the pressure. The pressure was determined by measuring the position of the stressed first-order Raman diamond edge[49]. Laser heating was performed above 120 GPa. X-ray diffraction patterns and radiometric temperature measurements were used to characterize the sample state *in situ*. Laser heating remained very local during this procedure, as our radiometric measurements and finite element calculations show. We did not expect any reaction with the gasket material (which remains close to room temperature during heating) or with the diamond anvils, and this was verified by subsequent X-ray diffraction and Raman mapping of the sample cavity including areas near the gasket edge. Raman measurements were performed using the 488, 532 and 660 nm lines of a solid-state laser. The laser probing spot dimension was 4 μm. Raman spectra were analysed with a spectral resolution of 4 cm^{-1} using a single-stage grating spectrograph equipped with a charge-coupled device (CCD) array detector. X-ray diffraction was measured in a double-sided laser heating system at the undulator XRD beamline at GeoSoilEnviroCARS, APS, Chicago, and the Extreme Conditions Beamline P02.2 at DESY (Germany), which have online laser heating capabilities. Temperature was determined spectroradiometrically. The X-ray probing beam size was ~2–5 μm in both beamlines.

References

1. Stevenson, D. J. Metallic helium in massive planets. *Proc. Natl Acad. Sci. USA* **105,** 11035–11036 (2008).
2. Huheey, J. E., Keiter, E. A., Keiter, R. L. & Medhi, O. K. *Inorganic Chemistry: Principles of Structure and Reactivity* (Harper & Row, 1983).
3. Hotop, H. & Lineberger, W. C. Binding energies in atomic negative ions: II. *J. Phys. Chem. Ref. Data* **14,** 731–750 (1985).
4. Hiby, J. W. Massenspektrographische untersuchungen an wasserstoff- und heliumkanalstrahlen (H_3^+, H_2^-, HeH$^+$, HeD$^+$, He$^-$). *Annalen der Physik* **426,** 473–487 (1939).
5. Wong, M. W. Prediction of a metastable helium compound: HHeF. *J. Am. Chem. Soc.* **122,** 6289–6290 (2000).
6. Grochala, W. On chemical bonding between helium and oxygen. *Pol. J. Chem.* **83,** 87–122 (2009).
7. Tariq, N., Taisan, N. A., Singh, V. & Weinstein, J. D. Spectroscopic detection of the LiHe molecule. *Phys. Rev. Lett.* **110,** 153201 (2013).
8. Loubeyre, P., Jean-Louis, M., LeToullec, R. & Charon-Gérard, L. High pressure measurements of the He-Ne binary phase diagram at 296 K: evidence for the stability of a stoichiometric Ne(He)$_2$ solid. *Phys. Rev. Lett.* **70,** 178–181 (1993).
9. Liu, H., Yao, Y. & Klug, D. D. Stable structures of He and H_2O at high pressure. *Phys. Rev. B* **91,** 014102 (2015).
10. Hermann, A. & Schwerdtfeger, P. Xenon suboxides stable under pressure. *J. Phys. Chem. Lett.* **5,** 4336–4342 (2014).
11. Zhu, Q. *et al.* Stability of xenon oxides at high pressures. *Nat. Chem.* **5,** 61–65 (2013).
12. Miao, M.-s. *et al.* Anionic chemistry of noble gases: formation of Mg–NG (NG = Xe, Kr, Ar) compounds under pressure. *J. Am. Chem. Soc.* **137,** 14122–14128 (2015).
13. Ma, Y. *et al.* Transparent dense sodium. *Nature* **458,** 182–185 (2009).
14. Zhang, W. *et al.* Unexpected stable stoichiometries of sodium chlorides. *Science* **342,** 1502–1505 (2013).
15. Lyakhov, A. O., Oganov, A. R. & Valle, M. in *Modern Methods of Crystal Structure Prediction* (ed. Oganov, A.R.) 147–180 (Wiley-VCH 2010).
16. Oganov, A. R. & Glass, C. W. Crystal structure prediction using ab initio evolutionary techniques: principles and applications. *J. Chem. Phys.* **124,** 244704 (2006).
17. Gerward, L. *et al.* X-ray diffraction investigations of CaF$_2$ at high pressure. *J. Appl. Crystallogr.* **25,** 578–581 (1992).
18. Gregoryanz, E. *et al.* Structural diversity of sodium. *Science* **320,** 1054–1057 (2008).
19. Hanfland, M., Loa, I. & Syassen, K. Sodium under pressure: bcc to fcc structural transition and pressure–volume relation to 100 GPa. *Phys. Rev. B* **65,** 184109 (2002).
20. Marqués, M. *et al.* Optical and electronic properties of dense sodium. *Phys. Rev. B* **83,** 184106 (2011).
21. Santamaría-Pérez, D., Mukherjee, G. D., Schwager, B. & Boehler, R. High-pressure melting curve of helium and neon: deviations from corresponding states theory. *Phys. Rev. B* **81,** 214101 (2010).
22. Gregoryanz, E., Degtyareva, O., Somayazulu, M., Hemley, R. J. & Mao, H.-k. Melting of dense sodium. *Phys. Rev. Lett.* **94,** 185502 (2005).
23. Somayazulu, M. *et al.* Pressure-induced bonding and compound formation in xenon–hydrogen solids. *Nat. Chem.* **2,** 50–53 (2010).
24. Miao, M.-S & Hoffmann, R. High pressure electrides: a predictive chemical and physical theory. *Acc. Chem. Res.* **47,** 1311–1317 (2014).
25. Miao, M.-S. & Hoffmann, R. High-pressure electrides: the chemical nature of interstitial quasiatoms. *J. Am. Chem. Soc.* **137,** 3631–3637 (2015).
26. Dye, J. L. Electrons as anions. *Science* **301,** 607–608 (2003).
27. Shannon, R. D. & Prewitt, C. T. Effective ionic radii in oxides and fluorides. *Acta Crystallogr. B* **25,** 925–946 (1969).
28. Rousseau, B. & Ashcroft, N. W. Interstitial electronic localization. *Phys. Rev. Lett.* **101,** 046407 (2008).
29. Pauling, L. The principles determining the structure of complex ionic crystals. *J. Am. Chem. Soc.* **51,** 1010–1026 (1929).
30. Bader, R. F. W. *Atoms in Molecules – A Quantum Theory* (Univ. Oxford Press, 1990).
31. Henkelman, G., Arnaldsson, A. & Jónsson, H. A fast and robust algorithm for Bader decomposition of charge density. *Comput. Mater. Sci.* **36,** 354–360 (2006).
32. Galeev, T. R., Dunnington, B. D., Schmidt, J. & Boldyrev, A. I. Solid state adaptive natural density partitioning: a tool for deciphering multi-center bonding in periodic systems. *Phys. Chem. Chem. Phys.* **15,** 5022–5029 (2013).
33. Zubarev, D. Y. & Boldyrev, A. I. Developing paradigms of chemical bonding: adaptive natural density partitioning. *Phys. Chem. Chem. Phys.* **10,** 5207–5217 (2008).
34. Dunnington, B. D. & Schmidt, J. R. Generalization of natural bond orbital analysis to periodic systems: applications to solids and surfaces via plane-wave density functional theory. *J. Chem. Theory Comput.* **8,** 1902–1911 (2012).
35. Foster, J. P. & Weinhold, F. Natural hybrid orbitals. *J. Am. Chem. Soc.* **102,** 7211–7218 (1980).
36. Dronskowski, R. & Blöchl, P. E. Crystal orbital Hamilton populations (COHP): energy-resolved visualization of chemical bonding in solids based on density-functional calculations. *J. Phys. Chem.* **97,** 8617–8624 (1993).
37. Andersen, O. K. & Jepsen, O. Explicit, first-principles tight-binding theory. *Phys. Rev. Lett.* **53,** 2571–2574 (1984).
38. Winzenick, M., Vijayakumar, V. & Holzapfel, W. B. High-pressure X-ray diffraction on potassium and rubidium up to 50 GPa. *Phys. Rev. B* **50,** 12381–12385 (1994).
39. Dye, J. L. Electrides: early examples of quantum confinement. *Acc. Chem. Res.* **42,** 1564–1572 (2009).
40. Vegas, Á. & Mattesini, M. Towards a generalized vision of oxides: disclosing the role of cations and anions in determining unit-cell dimensions. *Acta Crystallogr. B* **66,** 338–344 (2010).
41. Oganov, A. R. *et al.* Ionic high-pressure form of elemental boron. *Nature* **457,** 863–867 (2009).
42. Perdew, J. P., Burke, K. & Ernzerhof, M. Generalized gradient approximation made simple. *Phys. Rev. Lett.* **77,** 3865–3868 (1996).
43. Blöchl, P. E. Projector augmented-wave method. *Phys. Rev. B* **50,** 17953–17979 (1994).
44. Kresse, G. & Furthmüller, J. Efficiency of ab-initio total energy calculations for metals and semiconductors using a plane-wave basis set. *Comput. Mater. Sci.* **6,** 15–50 (1996).
45. Dovesi, R. *et al. CRYSTAL14 User's Manual* (Univ. of Torino, 2014).
46. Gatti, C., Saunders, V. R. & Roetti, C. Crystal field effects on the topological properties of the electron density in molecular crystals: the case of urea. *J. Chem. Phys.* **101,** 10686–10696 (1994).
47. Krier, G., Jepsen, O., Burkhardt, A. & Andersen, O. K. The TB-LMTO-ASA Program (Max-Planck-Institute for Solid State Research, 1995).
48. Togo, A., Oba, F. & Tanaka, I. First-principles calculations of the ferroelastic transition between rutile-type and CaCl$_2$-type SiO$_2$ at high pressures. *Phys. Rev. B* **78,** 134106 (2008).
49. Akahama, Y. & Kawamura, H. High-pressure Raman spectroscopy of diamond anvils to 250 GPa: method for pressure determination in the multimegabar pressure range. *J. Appl. Phys.* **96,** 3748–3751 (2004).
50. McMahon, J. M., Morales, M. A., Pierleoni, C. & Ceperley, D. M. The properties of hydrogen and helium under extreme conditions. *Rev. Mod. Phys.* **84,** 1607–1653 (2012).
51. Akahama, Y. & Kawamura, H. Pressure calibration of diamond anvil Raman gauge to 310 GPa. *J. Appl. Phys.* **100,** 043516 (2006).
52. Loubeyre, P. *et al.* Equation of state and phase diagram of solid ^{4}He from single-crystal X-ray diffraction over a large P–T domain. *Phys. Rev. Lett.* **71,** 2272–2275 (1993).
53. Shishkin, M. & Kresse, G. Self-consistent *GW* calculations for semiconductors and insulators. *Phys. Rev. B* **75,** 235102 (2007).

Author contributions

X.D. and A.R.O. designed the research. X.D., G.S. and I.A.P. performed and analysed the calculations. V.L.D. and R.D. carried out COHP analyses. A.G. designed experiments. S.L. and A.G. loaded the sample. A.F.G., E.S., S.L., V.B.P. and Z.K. performed the experiment. E.S. and A.F.G. analysed the experimental data. G.-R.Q., Q.Z., X.-F.Z. and A.I.B. assisted with calculations. All authors contributed to interpretation and discussion of the data. X.D., A.R.O., A.F.G., G.S., I.A.P., A.I.B. and H.-T.W. wrote the manuscript.

Additional information

Supplementary information is available in the online version of the paper. Reprints and permissions information is available online at www.nature.com/reprints. Correspondence and requests for materials should be addressed to A.R.O., X.F.Z. and H.T.W.

Competing financial interests

The authors declare no competing financial interests.